21PFL-0683

Three-Dimensional CFD Investigation of Pre-Spark Heat Release in a Boosted SI Engine

Author, co-author (Do NOT enter this information. It will be pulled from participant tab in MyTechZone)

Affiliation (Do NOT enter this information. It will be pulled from participant tab in MyTechZone

Abstract

Low-temperature heat release (LTHR) in spark-ignited internal combustion engines is a critical step toward the occurrence of auto-ignition, which can lead to an undesirable phenomenon known as engine knock. Hence, correct predictions of LTHR are of utmost importance to improve the understanding of knock and enable techniques aimed at controlling it. While LTHR is typically obscured by the deflagration following the spark ignition, extremely late ignition timings can lead to LTHR occurrence prior to the spark, i.e., pre-spark heat release (PSHR). In this research, PSHR in a boosted direct-injection SI engine was numerically investigated using three-dimensional computational fluid dynamics (CFD). A hybrid approach was used, based on the G-equation model for representing the turbulent flame front and the multi-zone well-stirred reactor model for tracking the chemical reactions within the unburnt region. A recently developed best practice was also employed which keeps the well-stirred reactor model active throughout the entire simulation. This allowed for correct predictions of the previous cycle trapped residuals which have a considerable effect on the onset of LTHR. Multi-cycle simulations were conducted using Co-Optima alkylate and E30 fuels. The predicted in-cylinder pressure and heat release rate agreed well with the experimental data and served as validation for the CFD model. Following the initial validation, the dynamics of PSHR was discussed and a series of parameters of interest were assessed. First, the effect of exhaust valve temperature was investigated, qualitatively highlighting the importance of boundary conditions uncertainty. Further analyses were carried out on the effects of fuel properties, including laminar flame speed (LFS) and heat of vaporization (HOV). The results indicate that PSHR phasing is slightly advanced with lower LFS as more trapped unburnt fuel is made available for the next cycle. A similar trend was observed with lower HOV as less intense spray cooling led to higher mixture temperatures, i.e., higher mixture reactivity. Finally, a comparison of Co-Optima alkylate and E30 fuels was made using the pressure-temperature trajectory framework. It was shown that the differences between Co-Optima alkylate and E30 in PSHR tendency are correlated with both HOV and chemical effects.

Introduction

The abnormal combustion phenomenon known as “engine knock”, i.e., the undesired auto-ignition process occurring in the end-gas during flame propagation, has been one of the major barriers towards developing high efficiency spark-ignition (SI) internal combustion engines (ICEs). Over this last century, numerous studies have been carried out to assess the mechanisms and factors influencing knock, but a detailed understanding is yet to be achieved. With recent developments in ICE downsizing and turbocharging, knock has become especially problematic due to higher power densities and more extreme thermodynamic condition in the cylinder [1].

Previous studies have revealed that knock is closely related to both engine operating conditions and fuel properties [2, 3]. A pioneering study by Leppard [4] identified a two-stage ignition process for alkanes, i.e., a first phase of low-temperature heat release (LTHR) followed by a high-temperature main-stage ignition. In more recent studies, it was revealed that LTHR has the potential to change the thermodynamic state of the end-gas and thus affect the engine’s knock behavior [5, 6]. Hence, understanding the likes of LTHR is critical for predicting the auto-ignition process. However, LTHR typically occurs in the end-gas after the spark, and its effect is therefore obscured by the heat release of the flame propagation. This results in obvious challenges that can make the experimental characterization of LTHR difficult.

Recent work by Szybist and Splitter [7], Splitter et al. [8], and Gilliam et al. [9] identified operating conditions for which LTHR occurs prior to spark timing. This pre-spark heat release (PSHR) was achieved with extreme late combustion phasing using low-octane sensitivity fuels. Due to the lack of temporal overlap between PSHR and flame propagation, the former can provide valuable experimental validation towards understanding LTHR. Splitter et al. showed that the exposure of PSHR, (i.e., exposure time to integrated inverse of ignition delay) increases with increased intake temperature and backpressure, while its occurrence is correlated to stochastic pre-ignition tendency and magnitude [10]. It is also known that the occurrence of PSHR could mitigate knock under high intake temperature conditions [8]. As far as fuel property effects are concerned, researchers have shown that the tendency of PSHR increases with lower octane sensitivity of the fuel [11]. To date, most studies have focused on fuel reactivity effects, while the effect of other important fuel properties, such as heat of vaporization (HOV) and laminar flame speed (LFS), has not been well explored, providing scientific justification for the current work.

In addition to several experimental studies on PSHR, numerical investigations have also been carried out to understand the chemistry and physics of PSHR in detail. DelVescovo et al. [12] utilized a two-zone SI engine model to determine whether literature kinetic mechanisms could accurately capture PSHR. The results showed that the selected four chemical mechanisms were not able to match experimental results adequately. If compared with zero-dimensional

(0-D) simulations, three-dimensional (3-D) computational fluid dynamics (CFD) simulations provide the advantage to take the mixture and thermal stratifications into account. These spatial non-uniformities have been proved to play an important role in direct-injection SI engines [13]. However, there have been no publications investigating PSHR using 3-D CFD simulations to date, justifying the motivation for this work.

This study presents a 3-D CFD investigation towards understanding PSHR in a boosted SI engine. The dynamics of PSHR are discussed first. Following, the effect of certain parameters such as exhaust valve temperature and fuel properties was analyzed. Finally, the learnings from the fuel property study were used to explain some of the differences in PSHR behavior between Co-Optima alkylate and E30, based upon their differences in chemical and physical characteristics.

Engine Specifications and Operating Condition

The engine platform used for the simulations performed in this work is a single-cylinder GM Ecotec LNF engine housed at Oak Ridge National Laboratory [7]. Bore and stroke are both 86.0 mm and the compression ratio is 9.2. The LNF engine features a direct-injection, side-mounted, production injector. The details of the engine specifications are listed in Table 1.

Table 1. Engine specifications.

Engine	GM Ecotec LNF
Bore/stroke [mm]	86.0/86.0
Connecting rod length [mm]	145.5
Crank offset [mm]	0.8
Compression ratio [-]	9.2:1
Fueling system	Direct injection, side-mounted

The operating condition discussed in this study is summarized in Table 2. The engine speed was 2000 rpm, with an air flow of 900 g/min and a stoichiometric air-to-fuel ratio. Boosted conditions were considered with an intake manifold pressure of 164 kPa and pressure difference of 8 kPa between intake and exhaust. The intake temperature was set at 90 °C. The injection pressure was 100 bar and the spark timing was 6 crank angle degrees (CAD) after top dead center (TDC).

Table 2. Details of the operating condition.

Engine speed [rpm]	2000
Air flow [g/min]	900
Fuel/air equivalence ratio [-]	1.0
Intake temperature [°C]	90
Intake pressure [kPa]	164
Manifold pressure difference [kPa]	8
Spark timing [CAD after TDC]	6
Injection pressure [bar]	100
Injection timing [CAD before TDC]	280
Exhaust gas recirculation [-]	0%

Two fuels were investigated, i.e., Co-Optima alkylate and E30, both among the "Co-Optima Core" fuels [14]. These two fuels are characterized by the same nominal research octane number (RON), but exhibit different octane sensitivity. The higher octane sensitivity for Co-Optima E30 is attributed to the high concentration of ethanol (30% by volume), which also resulted in a higher HOV if compared to the alkylate fuel. Some important properties of the two fuels are listed in Table 3.

Table 3. Properties of Co-Optima alkylate and E30, taken from Fouts et al. [14].

	ASTM Method	Co-Optima alkylate	Co-Optima E30
Research Octane Number	D2699	98.0	97.4
Motor Octane Number	D2700	96.6	86.6
Aromatics [vol%]	D1319	0	8.1
Saturates [vol%]	D1319	100	57.1
Olefins [vol%]	D1319	0	5
Ethanol [vol%]	D5599	<0.1	30.59
Density at 15 °C [kg/m³]	D4052	696.8	752.7
Lower heating value [MJ/kg]	D4809	44.524	38.170
Stoichiometric air-fuel ratio	NA	15.07	12.84
HOV [kJ/kg]	*	308	532

* Calculated from detailed hydrocarbon analysis, ASTM D6729

Modelling Approach and Validation

The CFD simulations were performed using the commercial code CONVERGE™, version 3.0 [15]. The computational domain, shown in Figure 1, consists of the cylinder, the intake port, and the exhaust port. The base mesh size was 2.0 mm. A fixed embedded refinement of 1 mm was applied to the entire cylinder region and a 0.25 mm minimum mesh size was applied near the spark plug gap. Adaptive mesh refinement of 0.5 mm was enabled where the sub-grid fluctuation of velocity magnitude and temperature were above 1.0 m/s and 2.5 K, respectively. The peak cell count for all cases was around 1.8 million.

All simulations relied on an unsteady Reynolds-averaged Navier-Stokes (RANS) formulation closed by the RNG k-ε turbulence model [16]. The fuel injection was modeled using a Lagrangian description of the spray, where the liquid fuel was injected as Lagrangian parcels [17] with their initial size equal to effective orifice diameter, i.e., 232 µm. The droplet breakup was modeled using the Kelvin-Helmholtz Rayleigh-Taylor model [18], while the drop collision was modeled with the no-time counter model [19]. The Frössling [20] and the O'Rourke [21] models were used to account for droplet evaporation and dispersion, respectively. The spray model was validated against experimental data of spray penetration and patternation collected in a constant volume vessel at Sandia National Laboratories. The details of the spray validation activity can be found in [22].

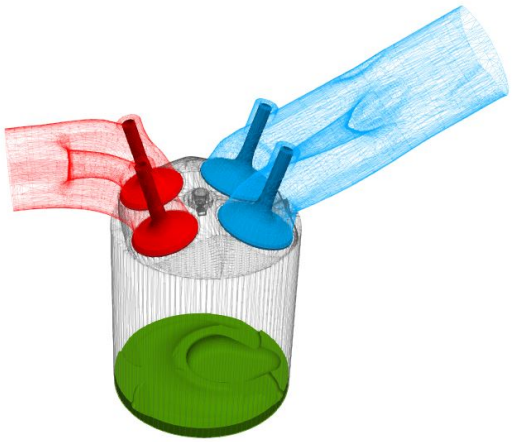

Figure 1. Computational domain of the single-cylinder LNF engine. Blue and red regions are the intake and exhaust manifolds, respectively. The top-surface of the piston is colored in green.

A hybrid approach was used to model the combustion process: the level-set G-equation model [23] was employed to track the propagation of the turbulent flame, while the well-stirred reactor model with detailed chemistry was used to model the reactions in the unburnt region. A tabular LFS model [24] was used for the calculation of the turbulent flame speed according to the following process. First, the CONVERGE one-dimensional solver was used to generate a look-up table of LFSs calculated for a range of temperatures, pressures, equivalence ratios, and exhaust gas recirculation ratios of interest. Then, the look-up table was used as input to the engine simulations so that the solver could interpolate the LFS table based on the local thermodynamic conditions. Finally, the turbulent flame speed was calculated using a turbulent burning velocity relationship [25] for RANS turbulence models. In order to capture the previous cycle trapped residuals correctly and due to their considerable effect on the onset of LTHR, the well-stirred reactor model was kept active throughout the entire simulation, which is different from common practices of ICE CFD modeling. A detailed description of this modeling approach can be found in [22]. As G-equation model was used in this study to track the turbulent flame propagation, the ignition was modeled as a sphere-shaped volume source with positive G value and a radius of 0.5 mm.

Two reaction mechanisms were used, i.e., a 121-species, 647-reactions reduced mechanism for Co-Optima alkylate and a 211-species, 1023-reactions reduced mechanism for Co-Optima E30. Both reductions were obtained from a comprehensive detailed kinetic mechanism for transportation fuels proposed by Lawrence-Livermore National Laboratory [26]. The fuel compositions proposed by Szybist et al. [27] were used, i.e., a four-component surrogate for Co-Optima alkylate and an eight-component one for Co-Optima E30. A multi-zone approach [28] was used to accelerate the chemical kinetic solver by grouping the computational cells with temperature bins of 5 K and equivalence ratio bins of 0.05. For all cases, open-cycle simulations were performed for 12 consecutive cycles. The first two cycles were discarded to ensure the effect of the initial conditions was removed. Therefore, only the results for the remaining ten cycles were used for the analysis. All the simulations were carried out on the Laboratory Computing Resource Center (LCRC) clusters at Argonne National Laboratory using 72 processors per single case, with a wall-clock time of approximately 28 hours per cycle.

The CFD setup was validated against experimental engine data reported in a previous study [7] and comparisons of in-cylinder pressure and apparent rate of heat release (AHRR) are shown in Figure 2. Under the operating condition investigated in this work, strong PSHR occurred for Co-Optima alkylate, while no PSHR was observed for Co-Optima E30. It is shown that the predicted in-cylinder pressure AHRR matched well with experiments in terms of both PSHR and post-spark pressure rise. The combustion phasing was also adequately captured. It is noted that although RANS simulations were performed, some of the cyclic variability was reasonably captured. This can be ascribed to the fact that cycle-to-cycle variability (CCV) in engines can be mainly attributed to the temporal variability of boundary conditions and amount of trapped in-cylinder residuals, as well as the chaotic nature of the flow [29]. Similar to what is discussed in Scarcelli et al [30], performing consecutive open-cycle simulations allowed to account for some of the intrinsic variability of boundary conditions and trapped residuals, which eventually led to the CCV observed in the simulations.

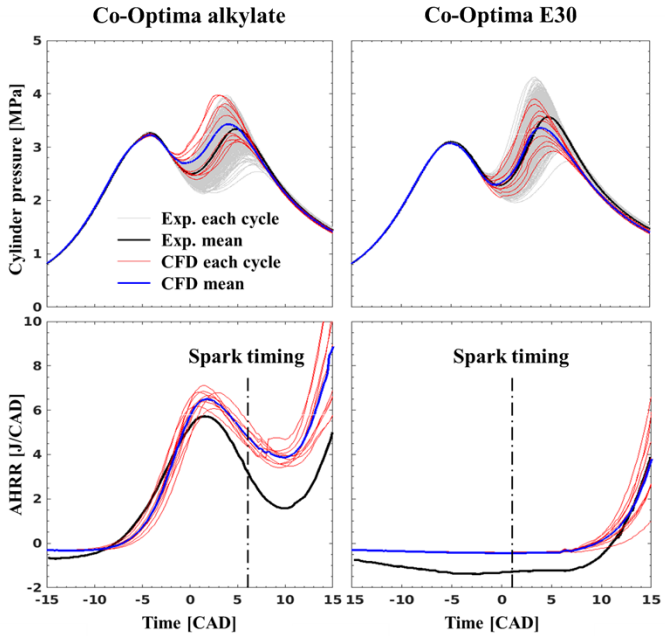

Figure 2. Experimental and predicted in-cylinder pressure and AHRR traces for Co-Optima alkylate and E30. Results of ten consecutive cycles are presented for each case.

Results and Discussion

This section consists of four parts. The dynamics of PSHR will be analyzed first using the validated simulation results of Co-Optima alkylate. Following, the effect of the T_{exh} boundary condition on the simulation results will be discussed. Afterwards, the focus will shift on the effect of fuel properties on PSHR. Finally, the difference between Co-Optima alkylate and E30 in terms of PSHR-related performance will be analyzed based on the fuels' differences in physical properties.

PSHR dynamics

The analysis of the PSHR dynamics is based on the simulation results obtained with Co-Optima alkylate, due to its propensity to show intense PSHR under the operating condition investigated in this work. Figure 3 illustrates the distributions of equivalence ratio, temperature, and formaldehyde mass fraction in the combustion chamber at three crankshaft positions before spark timing. For spatial reference, the

intake valves are located on the right side of each sub-plot, as marked on the top-right figure.

It can be observed that, despite a rather early injection (280 CAD before TDC), the in-cylinder mixture exhibited considerable stratification at the end of the compression stroke, with the fuel-air mixture being generally leaner near the intake valve side. Within the timeframe reported in Figure 3, the distribution of equivalence ratio remained relatively unchanged. At 10 CAD before TDC, the temperature field showed evident stratification with the fuel-rich region being generally cooler, due to a more intense spray cooling effect. At 5 CAD before TDC, due to higher mixture reactivity, evidence of low-temperature reactions was found in those locations characterized by higher local temperatures, which justified the observed temperature increase and generation of formaldehyde. At TDC, PSHR reached its peak, (cf. Figure 2), resulting in generalized temperature increase and formaldehyde production. These results indicated that mixture and thermal stratifications can have significant effect on the occurrence of PSHR whose onset occurs in higher-temperature, fuel-lean regions.

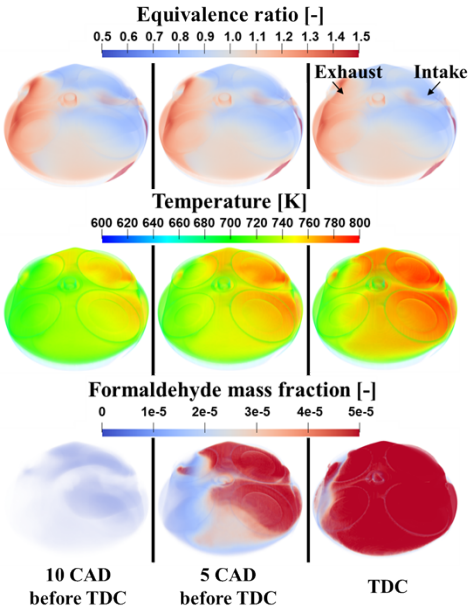

Figure 3. Temporal evolution of equivalence ratio, temperature, and formaldehyde mass fraction in the combustion chamber using Co-Optima alkylate.

Figure 4 shows a scatter plot progression of temperature versus equivalence ratio at several crank angles until spark timing. Each data point corresponds to each single computational cell. At 20 CAD before TDC, strong thermal and mixture stratification can be observed, with most of the cells contained within the 0.5-1.5 equivalence ratio range. 10 CAD later, the bulk temperature increased due to the compression, whereas the equivalence ratio distribution was relative unchanged. At 5 CAD before TDC, PSHR had just begun in the fuel-lean region with minor effects on the temperature increase. Between 5 CAD before TDC and TDC, a larger temperature increase was observed that extended toward the stoichiometric region of the scatterplots. Between TDC and the spark timing (6 CAD after TDC), the temperature increased significantly in the fuel-rich mixtures, while the temperature in the fuel-lean region did not show substantial changes, suggesting the completion of PSHR reactions in the fuel-lean region and their transition to the fuel-rich region. Also, it should be noted that the magnitude of the temperature increment caused by PSHR was larger in the fuel-rich region. This is explained by the larger amount of fuel in the high equivalence ratio region, which intuitively results in higher chemical potential, and thus more heat available to be released. Moreover, it was found that the temperature increment was limited to ~820 K, independent of the equivalence ratio. As it will be shown later in this manuscript, ~820 K is the temperature at which first-stage, LTHR reactions end for Co-Optima alkylate.

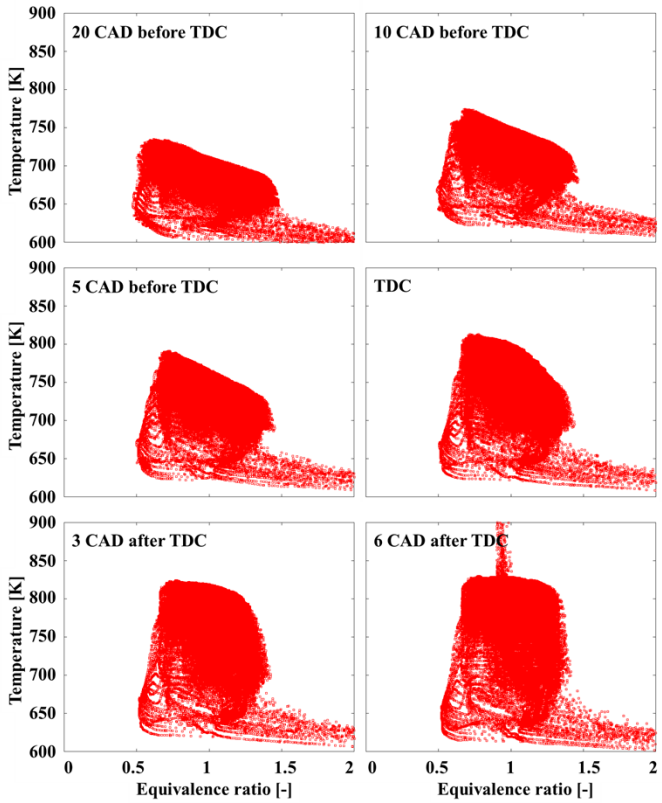

Figure 4. Scatter plots of temperature versus equivalence ratio at the indicated crank angles using Co-Optima alkylate.

Effect of Exhaust Valve Temperature

In all the simulations presented in this manuscript, the wall temperature of the combustion chamber was set to 450 K based on considerations of trapped mass and heat transfer during the compression and expansion strokes. On the other hand, an accurate estimate from experiments is unavailable and experience dictates that T_{exh} should be higher than the temperature of other in-cylinder locations [31]. To understand how T_{exh} impacts the predictions of PSHR, three cases with three different T_{exh} were simulated and the results are discussed in this subsection using Co-Optima alkylate.

Figure 5 shows of equivalence ratio and temperature distributions at three different crankshaft positions for the three cases, with T_{exh} of 450, 550, and 650 K. It was found that the mixture distribution changed moderately as T_{exh} was varied. However, the fuel-rich mixture was still located near the exhaust valve side (right). Furthermore, if analyzed individually, all cases showed no significant change in the distribution of equivalence ratio within the timeframe discussed.

In terms of the temperature distribution, higher T_{exh} resulted in higher local temperatures not only on the exhaust side, but also on the intake side. This is because this engine is characterized by considerable tumble flow under the conditions investigated here. Despite the large increases in T_{exh}, PSHR continued to begin in the fuel-lean region near the intake valve, which is the same observation made with a constant wall temperature in Figure 3. The increase in T_{exh} did cause some other differences in the simulation, though. The gas temperature was found to be higher with higher T_{exh} at 10 CAD before TDC, when PSHR had not yet begun. This was observed not only near the exhaust valve but also in the other locations closer to the intake valves. At 5 CAD before TDC as well as at TDC, the onset of PSHR resulted in the increase of the overall in-cylinder temperature. This temperature increment induced by PSHR was stronger with higher T_{exh}, possibly due to the higher bulk gas temperature.

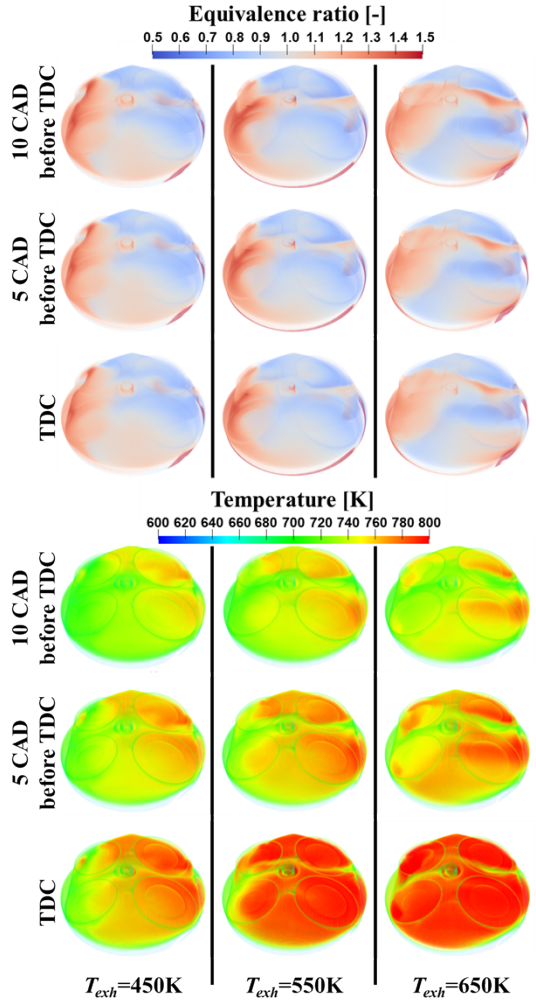

Figure 5. Distributions of equivalence ratio (top) and temperature (bottom) at several crank angles for the three cases with different T_{exh}.

Figure 6 shows the predicted in-cylinder pressure and AHRR traces for the three cases. For each case, the results of ten consecutive cycles are plotted. No major differences were observed in terms of T_{exh}'s effect on in-cylinder pressure behavior as shown in the pressure trace plots. In Figure 6 (right), it is shown that the higher T_{exh} resulted in slightly advanced PSHR phasing, while the magnitude of PSHR was not affected much. This is consistent with the trends observed in Figure 5. Overall, the results reported in this subsection indicate that, despite the wide range investigated, T_{exh} impacted gas temperature distributions and PSHR phasing only slightly. Therefore, for the PSHR conditions analyzed in this work, the choice to use the same wall temperature for all in-cylinder surfaces can be considered as a reasonable simplified assumption for setting up the wall temperatures.

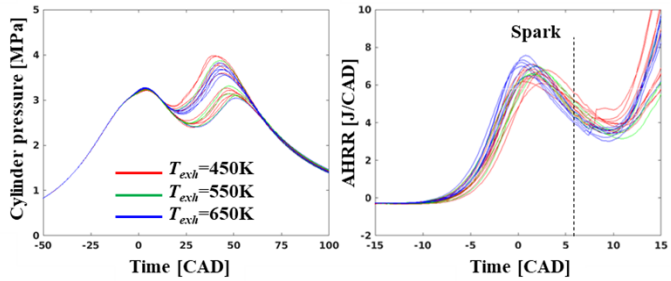

Figure 6. Predicted AHRR traces for the three cases with different T_{exh}. Results are reported for ten consecutive cycles for each case.

Fuel property effects

This subsection focuses on the effect on PSHR of two important fuel properties that affect fuel phase change and flame propagation, i.e., HOV and LFS. This study was performed by artificially changing said properties. The goal is to gain understanding about how similar fuels with slightly different properties behave under nominally identical operating conditions. Figure 7 shows the effect of HOV on the predicted in-cylinder pressure and AHRR traces for ten consecutive cycles. Three cases are discussed here: the Baseline case corresponds to the one with the original properties of Co-Optima alkylate (cf. Figure 2), while the other two have heats of vaporization that are respectively 30% higher and lower than the original value across the entire temperature range for which this property is defined. The in-cylinder pressure reported in Figure 7 (left) indicate that the post-spark pressure rise connected to the main-stage flame propagation was not affected much by the changes in HOV. Moreover, with lower HOV, the phasing of PSHR was slightly advanced, while its magnitude was not affected much, as confirmed by the AHRR traces in Figure 7 (right). This can be explained by the less intense spray cooling effect due to the lower HOV, which in turn resulted in overall slightly higher gas temperature and fuel-air mixture reactivity.

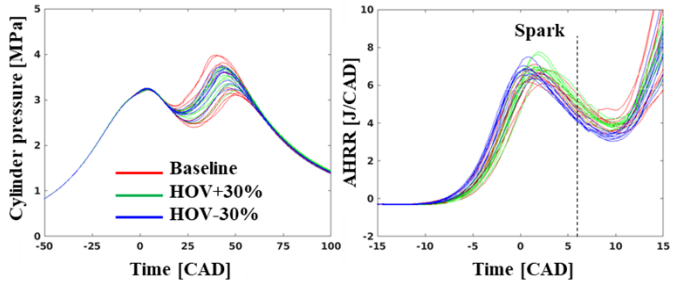

Figure 7. Effect of HOV on the predicted in-cylinder pressure and AHRR traces. Results of ten consecutive cycles are presented for each case.

In order to understand the relationship between PSHR and the fuel's chemical reactivity, the pressure-temperature (P-T) trajectory framework was combined with maps of constant volume ignition delays [32]. Figure 8 shows the P-T trajectory until TDC for the three cases with different HOV, overlapped with the ignition delay contours of Co-Optima alkylate. The P-T trajectories are obtained by extracting

the average temperature and pressure in the combustion chamber and averaging these values over the ten consecutive cycles. The first-stage ignition delay (cf. Figure 8 (left)) is closely related to LTHR and is defined as the time at which the first derivative of temperature with respect to time is maximum. The main-stage ignition delay is plotted on the right of Figure 8 and is defined as the time required for the temperature to increase by 400 K from its initial value. The ignition delays were calculated using CHEMKIN-Pro [33].

It was found that the main-stage ignition delay is relatively large during compression (above 5.0 ms, corresponding to 60 CAD), while the first-stage ignition delay was much shorter. PSHR began when the thermodynamic state intersected the 2.0 ms first-stage ignition delay isoline, confirmed by the P-T trajectory being pushed toward higher temperatures as a result of the LTHR [7]. Figure 8 also shows that, with higher HOV, the P-T trajectory was slightly shifted toward the left side, indicating slightly lower bulk gas temperature. This less reactive thermodynamic state resulted in longer first-stage ignition delay, which explains the delay in PSHR phasing.

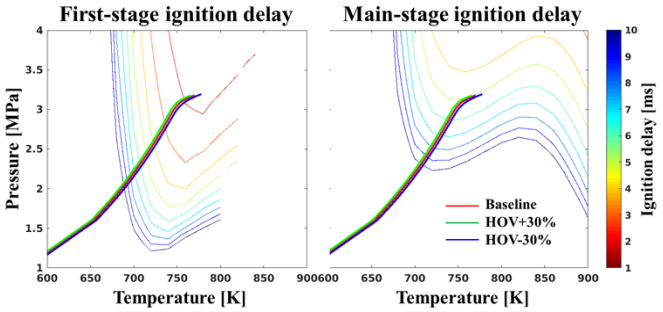

Figure 8. Effect of HOV on the P-T trajectory until TDC, combined with the first-stage (left) and main-stage (right) ignition delay maps.

Figure 9 shows the effect of LFS on the predicted in-cylinder pressure and AHRR traces using ten consecutive cycles. Three cases are discussed and, consistent with the HOV study, the baseline case is the same reported in Figure 2. The other two cases are characterized by LFSs that are respectively 30% higher and 30% lower than the original values across the entire ranges of pressure, temperature, and equivalence ratios. The results indicate that the pressure rise due to the main-stage flame propagation was faster for the case with higher LFS, as expected. On the other hand, it was also revealed that the PSHR phasing was slightly advanced with lower LFS, which might seem surprising as PSHR occurs ahead of the spark and flame propagation. A plausible explanation to this interesting phenomenon is likely given by the effect of trapped residuals from the previous cycle. Specifically, as the LFS decreases, the combustion efficiency is expected to decrease accordingly. This can result in more non-fully burnt intermediate species and radicals that are left lingering in the combustion chamber for the next cycle. Therefore, in the following cycle, these residuals facilitate the occurrence of PSHR by slightly increasing the reactivity of the fuel-air mixture, thus resulting in marginally advanced PSHR.

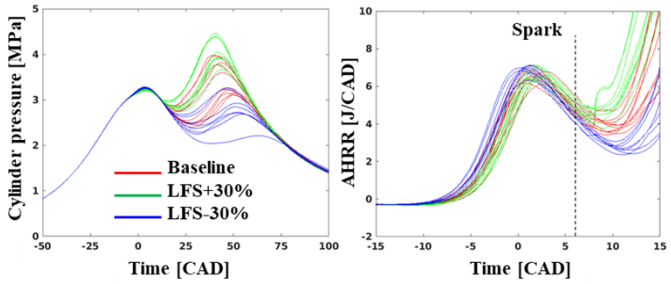

Figure 9. Effect of LFS on the predicted in-cylinder pressure and AHRR traces. Results of ten consecutive cycles are presented for each case.

For the low speed boosted operating point analyzed in this work, the valve overlap was 27 CAD, which is small enough to expect non-negligible amounts of trapped residuals due to a limited scavenging effect. To confirm this statement and to demonstrate the effect of trapped residuals, an additional simulation was performed using a CONVERGE feature called “skip species” which allows to eliminate the trapped residuals after the end of combustion in each cycle. As shown in Figure 10 when such feature is used no PSHR is predicted, which corresponds to a configuration without trapped residuals. This is a clear indication that the trapped residuals facilitate the onset of PSHR significantly, supporting the explanation provided above about the effect of LFS.

Figure shows the P-T trajectory until TDC for the three cases with different LFSs, overlaid onto the ignition delay contours of Co-Optima alkylate. Differently than with HOV, it was found that the LFS had minor effects on the P-T trajectory. However, as shown in Figure 9, the PSHR phasing was considerably advanced with lower LFS. Even though the thermodynamic state was similar, the reactivity of the mixture was enhanced for the case with lower LFS, because of the trapped residuals from each previous cycle. However, the change in reactivity could not be observed by means of the ignition delay contours as only stoichiometric fuel-air mixtures are considered when calculating ignition delays.

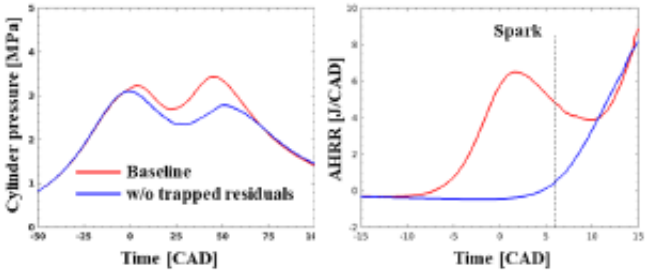

Figure 10. Effect of trapped residuals on the predicted in-cylinder pressure and AHRR traces.

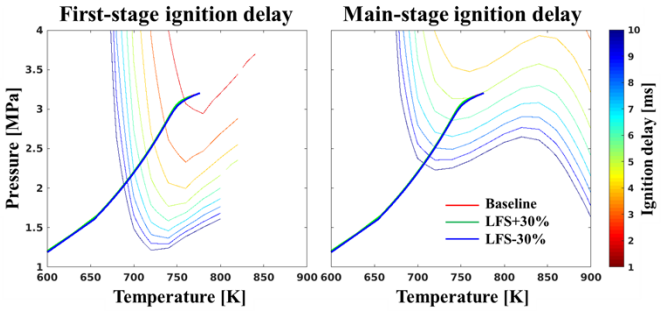

Figure 11. Effect of LFS on the PT trajectory until TDC, combined with the first-stage (left) and main-stage (right) ignition delay maps.

Comparison between Co-Optima Alkylate and E30

In this final subsection, the Co-Optima alkylate and E30 fuels are directly compared in terms of their PSHR performance. As shown in Figure 10, the P-T trajectories of the two fuels are illustrated. The P-T trajectories are obtained by extracting the average temperature and pressure in the combustion chamber and averaging these values over the ten consecutive cycles.

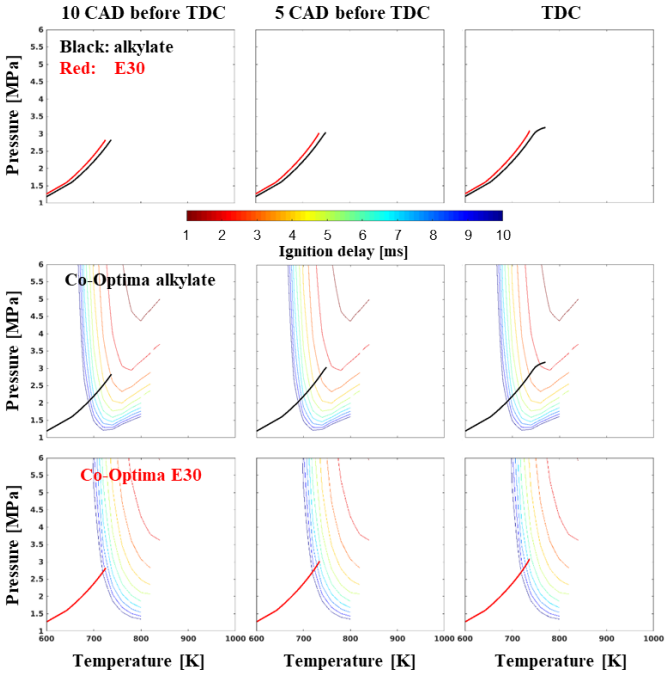

Figure 10. P-T trajectory analysis for Co-Optima Alkylate and E30 fuels. Top row: side-by-side comparison of P-T trajectories for the two fuels. Middle row: P-T trajectory of Co-Optima alkylate overlaid onto its first-stage ignition delay contour; Bottom row: P-T trajectory of Co-Optima E30 overlaid onto its first-stage ignition delay contour.

It is noted that under the condition investigated in this work, strong PSHR occurred for the alkylate fuel while no PSHR was observed for Co-Optima E30, as illustrated in Figure 2. It was found that the P-T trajectory of Co-Optima alkylate was always on the right side of that of Co-Optima E30. This is mainly attributed to the lower HOV of Co-Optima Alkylate. At 10 and 5 CAD before TDC, PSHR is not yet significant for Co-Optima alkylate. Therefore, the in-cylinder pressure for the two fuels was similar at the same crankshaft positions. At TDC, as a result of PSHR, Co-Optima alkylate exhibited not only higher temperature but also higher pressure.

Figure 13 illustrates the P-T trajectory of Co-Optima alkylate and E30 in the fuel-lean region overlaid onto the corresponding first-stage ignition delay map at the equivalence ratio (φ) of 0.6. The pressure and temperature were averaged within the equivalence ratio range from 0.4 to 0.8 and over the ten consecutive cycles. The P-T trajectory in the fuel-lean region is discussed because PSHR occurs at first in this region, as illustrated in Figure 3.

From a chemistry perspective, the first-stage ignition delay maps indicated that Co-Optima alkylate was characterized by much stronger reactivity in the low-temperature regime. The combination of HOV and chemical effects was such that a much more intense LTHR was observed with Co-Optima alkylate during the final stages of the compression stroke. At TDC, the first-stage ignition delay of the alkylate fuel is about 2.0 ms, while the same quantity is around 5.0 ms for Co-Optima E30. These results revealed that the difference in PSHR behavior between Co-Optima alkylate and E30 was correlated with both HOV and chemical effects.

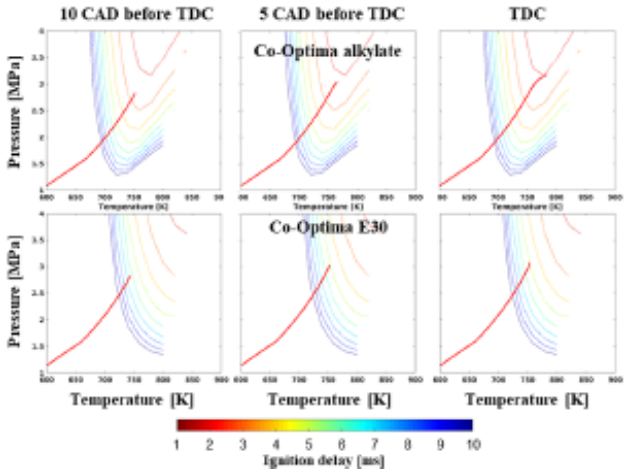

Figure 13. Top: P-T trajectory of Co-Optima alkylate in the fuel-lean region (0.4< φ<0.8) overlaid onto its first-stage ignition delay contour at φ=0.6; Bottom: P-T trajectory of Co-Optima E30 in the fuel-lean region (0.4< φ<0.8) overlaid onto its first-stage ignition delay contour at φ=0.6.

Summary

In this study, computational fluid dynamics (CFD) simulations were performed to study the pre-spark heat release (PSHR) in a boosted direct-injection spark-ignited engine. The dynamics of PSHR were revealed, and the effect of exhaust valve temperature (T_{exh}), heat of vaporization (HOV), and laminar flame speed (LFS) were discussed. Finally, the differences in PSHR behavior between Co-Optima alkylate and E30 fuels were reported.

The key take-away points of this study can be summarized as follow:

1. PSHR began within the fuel-lean mixtures where gas temperature was higher due to less intense spray cooling. However, its overall effect on the local thermodynamic states was more significant in the fuel-rich mixtures due to higher chemical potential. PSHR was observed to end concurrently with the end of low-temperature reactions.

2. Higher T_{exh} resulted in generally higher bulk gas temperature and slightly advanced PSHR phasing. As the effect was not very significant, the assumption of constant wall temperature across the entire combustion chamber proved to be reasonable for accurate predictions of PSHR.
3. Higher HOV resulted in more intense spray cooling effect, which in turn caused the bulk gas temperature to decrease, leading to delayed PSHR phasing.
4. Changes in LFS did not affect the in-cylinder P-T trajectory significantly. However, lower LFSs resulted in higher concentrations of trapped residuals from the previous cycle, which enhanced the mixture reactivity and propensity to show advanced PSHR phasing.
5. Under the condition studied, stronger PSHR was observed for Co-Optima alkylate, while no PSHR occurred for Co-Optima E30. The CFD setup proposed in this work was able to capture this difference correctly. The different behavior was mainly attributed to the lower HOV and higher low-temperature reactivity of Co-Optima alkylate.

References

1. Jo, Y.S., Bromberg, L., and Heywood, J.B., "Optimal Use of Ethanol in Dual Fuel Applications: Effects of Engine Downsizing, Spark Retard, and Compression Ratio on Fuel Economy," *SAE International Journal of Engines* 9(2):1087-1101, 2016, doi: 10.4271/2016-01-0786.
2. Kalghatgi, G.T., "Fuel Anti-Knock Quality - Part I. Engine studies," SAE Technical Paper 2001-01-3584, 2001, doi: 10.4271/2001-01-3584.
3. Yue, Z. and Som, S., "Fuel Property Effects on Knock Propensity and Thermal Efficiency in a Direct-Injection Spark-Ignition Engine," *Applied Energy* 114221, 2019, (in press, available online), doi: 10.1016/j.apenergy.2019.114221.
4. Leppard W.R., "The Chemical Origin of Fuel Octane Sensitivity," SAE Technical Paper 902137, 1990, doi: 10.4271/902137.
5. Vuilleumier, D. and Sjöberg, M., "Significance of RON, MON, and LTHR for Knock Limits of Compositionally Dissimilar Gasoline Fuels in a DISI Engine," *SAE International Journal of Engines* 10(3):938-950, 2017, doi: 10.4271/2017-01-0662.
6. Kim, N., Vuilleumier, D., Sjöberg, M., Yokoo, N., Tomoda, T., and Nakata, K., "Using Chemical Kinetics to Understand Effects of Fuel Type and Compression Ratio on Knock-Mitigation Effectiveness of Various EGR Constituents," *SAE International Journal of Advances and Current Practices in Mobility* 1(4):1560-1580, 2019, doi: 10.4271/2019-01-1140.
7. Szybist, J.P. and Splitter, D.A., "Understanding Chemistry-Specific Fuel Differences at a Constant RON in a Boosted SI Engine," *Fuel* 217:370-381, 2018, doi: 10.1016/j.fuel.2017.12.100.
8. Splitter, D.A., Gilliam, A., Szybist, J.P., and Ghandhi, J.B., "Effects of Pre-Spark Heat Release on Engine Knock Limit," *Proceedings of the Combustion Institute* 37(4):4893-4900, 2019, doi: 10.1016/j.proci.2018.05.145.
9. Gilliam, A., Splitter, D.A., Szybist, J.P., Ghandhi, J.B., "Fuel Kinetic Effects on Pre-Spark Heat Release and Engine Knock Limit," *THIESEL Conference on Thermo- and Fluid Dynamic Processes in Direct Injection Engines*, Valencia, Spain, 2018.
10. Splitter, D.A., Kaul, B., Szybist, J.P., and Jatana, G.S., "Engine Operating Conditions and Fuel Properties on Pre-Spark Heat Release and SPI Promotion in SI Engines," *SAE International Journal of Engines* 10(3):1036-1050, 2017, doi: 10.4271/2017-01-0688.
11. Szybist, J.P. and Splitter D.A., "Pressure and Temperature Effects on Fuels with Varying Octane Sensitivity at High Load in SI Engines," *Combustion and Flame* 177:49-66, 2017, doi: 10.1016/j.combustflame.2016.12.002.
12. DelVescovo, D.A., Splitter, D.A., Szybist, J.P., and Jatana, G.S., "Modeling Pre-Spark Heat Release and Low Temperature Chemistry of Iso-Octane in a Boosted Spark-Ignition Engine," *Combustion and Flame* 212:39-52, 2020, doi: 10.1016/j.combustflame.2019.10.009.
13. Adomeit, P., Lang, O., Pischinger, S., Aymanns, R., Graf, M., and Stapf, G., "Analysis of cyclic fluctuations of charge motion and mixture formation in a DISI engine in stratified operation," SAE Technical Paper 2007-01-1412, 2007, doi: 10.4271/2007-01-1412.
14. Fouts, L.A., Fioroni, G.M., Christensen, E.D., Ratcliff, M.A., McCormick, R.L., Zigler, B.T., Sluder,S., Szybist, J.P., Dec, J.E., Miles, P.C., Ciatti, S., Bays, J.T., Pitz, W., and Mehl, M., "Co-Optimization of Fuels & Engines: Properties of Co-Optima Core Research Gasolines," National Renewable Energy Laboratory, Technical Report NREL/TP-5400-71341, Golden, 2018.
15. Richards, K.J., Senecal, P.K., and Pomraning E., "CONVERGE 3.0 Manual," Convergent Science, Inc., Madison, WI, USA, March 2020.
16. Yakhot, V., Orszag, S.A., Thangam, S., Gatski, T.B., and Speziale, C.G., "Development of Turbulence Models for Shear Flows by a Double Expansion Technique," *Physics of Fluids A: Fluid Dynamics* 4(7):1510-1520, 1992, doi: 10.1063/1.858424.
17. Reitz, R.D., "Modeling Atomization Processes in High-Pressure Vaporizing Sprays," *Atomisation and Spray Technology*, 3(4):309-337, 1987.
18. Beale, J.C. and Reitz, R.D., "Modeling Spray Atomization with the Kelvin-Helmholtz/Rayleigh-Taylor Hybrid Model," *Atomization and Sprays*, 9(6):623-650, 1999, doi: 10.1615/AtomizSpr.v9.i6.40.
19. Schmidt, D.P. and Rutland, C.J., "A New Droplet Collision Algorithm," *Journal of Computational Physics*, 164(1):62-80, 2000, doi: 10.1006/jcph.2000.6568.
20. Amsden, A.A., "KIVA-3V: A Block Structured KIVA Program for Engines with Vertical or Canted Valves," Los Alamos National Laboratory, Technical Report No. LA-13313-MS, 1997.
21. Amsden, A.A., O'Rourke, P.J., and Butler, T.D., "KIVA-II: A Computer Program for Chemically Reactive Flows with Sprays," Los Alamos National Laboratory, Technical Report LA-11560-MS, 1989.
22. Guo, H., Torelli, R., Szybist, J.P., Som, S., "CFD Modeling of Pre-Spark Heat Release in a Boosted Direct-Injection Spark-Ignition Engine," *under preparation*.
23. Pitsch, H., "A G-Equation Formulation for Large-Eddy Simulation of Premixed Turbulent Combustion," *Center for Turbulence Research Annual Research Briefs*, 2002.
24. Pal, P., Wu, Y., Lu, T., Som, S., See, Y. C., and Le Moine, A., "Multidimensional Numerical Simulations of Knocking Combustion in a Cooperative Fuel Research Engine," *Journal of Energy Resources Technology*, 140(10):102205-1-8, 2018, doi: 10.1115/1.4040063.
25. Peters, N., "Turbulent Combustion," Cambridge University Press, Cambridge, UK, 2000, doi: 10.1017/CBO9780511612701.
26. Mehl, M., Wagnon, S., Tsang, L., Kukkadapu, G., Pitz, W.J., Westbrook, C.K., Tsang, Y., Curran, H.J., Atef, N., Rachidi, M.A., Sarathy, M.S., and Ahmed, A., "A Comprehensive Detailed Kinetic Mechanism for the Simulation of Transportation Fuels," *10th U.S. National Combustion Meeting*, Park College, MD, USA, 2017.
27. Szybist, J.P., Wagnon, S.W., Splitter, D.A., Pitz, W.J., and Mehl, M., "The Reduced Effectiveness of EGR to Mitigate Knock at

High Loads in Boosted SI Engines," *SAE International Journal of Engines* 10(5):2305-2318, 2017, doi: 10.4271/2017-24-0061.
28. Babajimopoulos, A., Assanis, D.N., Flowers, D.L., Aceves, S.M., and Hessel, R.P., "A Fully Coupled Computational Fluid Dynamics and Multi-Zone Model With Detailed Chemical Kinetics for the Simulation of Premixed Charge Compression Ignition Engines," International Journal of Engine Research, 6(5):497-512, 2005, doi: 10.1243/146808705X30503.
29. Probst, D., Wijeyakulasuriya, S., Pal, P., Kolodziej, C., and Pomraning, E., "Accelerating Computational Fluid Dynamics Simulations of Engine Knock Using a Concurrent Cycles Approach," *Proceedings of the ASME 2020 Internal Combustion Engine Fall Technical Conference*, ASME ICEF2020-2916, 2020, doi: 10.1115/ICEF2020-2916.
30. Scarcelli, R., Richards, K., Pomraning, E., Senecal, P.K., Wallner, T., and Sevik, J., "Cycle-to-Cycle Variations in Multi-Cycle Engine RANS Simulations," SAE Technical Paper 2016-01-0593, 2016, doi: 10.4271/2016-01-0593.
31. Yue, Z., Edwards, K.D., Sluder, C.S., and Som, S., "Prediction of Cyclic Variability and Knock-Limited Spark Advance in a Spark-Ignition Engine," *Journal of Energy Resources Technology*, 141(10):102201-1-8, 2019, doi: 10.1115/1.4043393.
32. Szybist, J.P. and Splitter D.A., "Impact of engine pressure-temperature trajectory on autoignition for varying fuel properties," *Applications in Energy and Combustion Science* 1-4:100003, 2020, doi: 10.1016/j.jaecs.2020.100003.
33. CHEMKIN-PRO 15141, Reaction Design, San Diego, 2015.

Contact Information

Hengjie Guo, Ph.D.
Postdoctoral Researcher
Argonne National Laboratory
9700 S Cass Avenue, Building 362
Lemont, IL 60439-4801, USA
E-mail: hengjie.guo@anl.gov

Roberto Torelli, Ph.D.
Research Scientist
Argonne National Laboratory
9700 S Cass Avenue, Building 362
Lemont, IL 60439-4801, USA
E-mail: rtorelli@anl.gov

Acknowledgments

The submitted manuscript has been created by UChicago Argonne, LLC, Operator of Argonne National Laboratory (Argonne). Argonne, a U.S. Department of Energy (DOE) Office of Science laboratory, is operated under Contract No. DE-AC02-06CH11357. The U.S. Government retains for itself, and others acting on its behalf, a paid-up nonexclusive, irrevocable worldwide license in said article to reproduce, prepare derivative works, distribute copies to the public, and perform publicly and display publicly, by or on behalf of the Government. This research was conducted as part of the Co-Optimization of Fuels and Engines (Co-Optima) initiative sponsored by the US Department of Energy Office of Energy Efficiency and Renewable Energy and Bioenergy Technologies and Vehicle Technologies Offices.

The authors wish to thank:

1. Kevin Stork, Gurpreet Singh, and Michael Weismiller, program managers at DOE, for their support through the Co-Optima initiative.
2. Krishna Kalvakala and Pinaki Pal at Argonne for their help with the 0-D simulations.
3. Lyle Pickett at Sandia National Laboratories for providing the spray experimental data.
4. LCRC cluster facilities at Argonne for computing resource on the Bebop cluster.
5. Convergent Science Inc., for providing the CONVERGE CFD software licenses.

Abbreviations and Definitions

0-D	Zero-dimensional
3-D	Three-dimensional
AHRR	Apparent heat release rate
CAD	Crank angle degree
CCV	Cycle-to-cycle variability
CFD	Computational fluid dynamics
HOV	Heat of vaporization
ICE	Internal combustion engine
LCRC	Laboratory Computing Resource Center (at Argonne National Laboratory)
LFS	Laminar flame speed
LTHR	Low-temperature heat release
PSHR	Pre-spark heat release
P-T	Pressure-temperature (trajectory)
RANS	Reynolds-averaged Navier-Stokes
SI	Spark-ignition (or spark-ignited)
TDC	Top dead center
T_{exh}	Exhaust valve temperature